

# Study on Toughening Phenolic Foams in Phosphorus-Containing Tung Oil-Based Derivatives

Fei Song<sup>1</sup>, Puyou Jia<sup>1,\*</sup>, Yanan Xiao<sup>2</sup>, Caiying Bo<sup>1</sup>, Lihong Hu<sup>1</sup> and Yonghong Zhou<sup>1,\*</sup>

<sup>1</sup>Institute of Chemical Industry of Forest Products, Chinese Academy of Forestry (CAF); National Engineering Laboratory for Biomass Chemical Utilization; Co-Innovation Center of Efficient Processing and Utilization of Forest Resources; Key Laboratory of Chemical Engineering of Forest Products, National Forestry and Grassland Administration; Key Laboratory of Biomass Energy and Materials, Nanjing, 210042, China.

<sup>2</sup>School of Petroleum and Chemical Engineering, Dalian University of Technology, Dalian, 124221, China.

\*Corresponding Authors: Yonghong Zhou. Email: yhzhou777@sina.com; Puyou Jia. Email: jiapuyou@icifp.cn.

**Abstract:** Phenolic foams (PFs) as thermal insulation material with outstanding flame retardancy are required to match society's ever-expanding safety expectations; however, a trade-off exists between flame retardancy and toughness. Here, for the first time, we synthesized a novel reactive phosphorus-containing tung-oil-based derivative and used it to toughen PF, resulting in PFs with a combination of excellent mechanical properties and flame retardancy. Compared with pure PF, the modified PFs exhibit enhanced mechanical properties, with specific compressive and flexural strengths as high as 5.67 MPa and 12.46 MPa, which represent increases of 90.67% and 178.7% over those of pure PF, respectively. Meanwhile, the limiting oxygen index (LOI) values of the modified PFs are improved as much as 40.83%. Scanning electron microscopy micrographs show that the microstructure of the modified PFs is better than that of pure PF, with a more uniform cell morphology, a narrower pore size distribution range, and a smaller average pore size, all of which are beneficial to the foam's mechanical properties. This study provides a scientific paradigm for the development of advanced PFs based on renewable biological resources.

**Keywords:** Tung oil; phenolic foams; toughen; mechanical properties; LOI

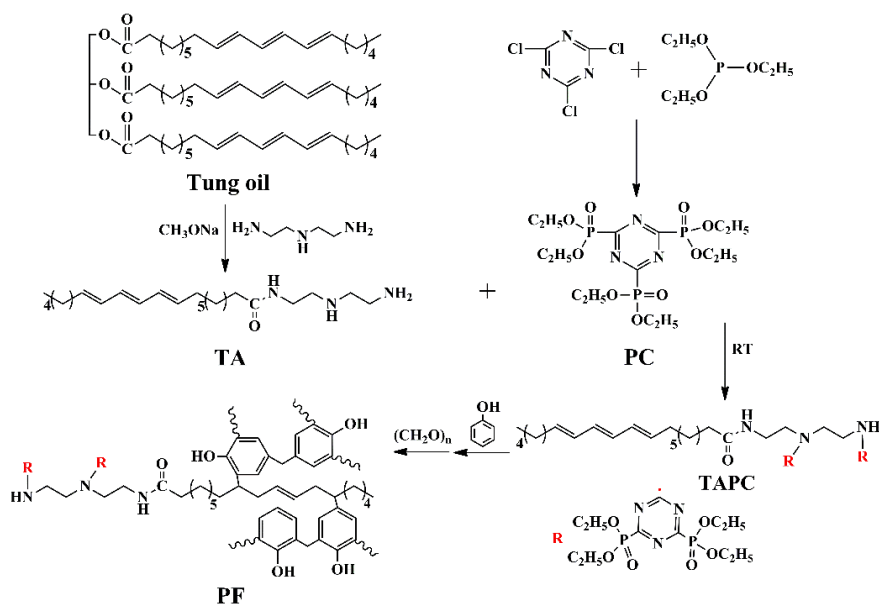
## 1 Introduction

Because of their flammability, tendency to generate of large amounts of highly toxic fumes, and tendency to drip during combustion, conventional thermal insulation foams (e.g., polystyrene [1] and polyurethane [2]) are increasingly unable to meet the strict safety requirements being imposed worldwide [3,4]. As third-generation insulation, phenolic foams (PFs) exhibit excellent fire performance, including good flame retardancy, low smoke production and no dripping during combustion, low smoke toxicity, and resistance to flame penetration [5-7]. However, because the aromatic ring of PFs is only crosslinked by methylene, these foams exhibit poor mechanical properties, including poor toughness and high pulverization rates, which severely limits their range of application [8,9]. An efficient toughening method to overcome this problem is the introduction of flexible long chains into the rigid network of PFs through chemical modification [10,11]. Unfortunately, the presence of flexible chains tends to adversely affect the flame retardancy of PFs, which hinders their application as a fire-resistant material [12,13]. Therefore, the flame retardancy of the toughener should be improved. Compared with other flame-retardant elements, phosphorus has higher flame-retardant efficiency because of the high flame retardancy of both its gas phase and condensed phase [14]. Moreover, compared with halogen flame retardants, which produce strong carcinogens and corrosive gases during decomposition, phosphorus-containing flame retardants are environmentally friendly and have thus attracted intensive interest [15].

The vast majority of existing toughening agents are derived from petroleum resources. In the global

context of the petroleum shortage crisis and green sustainable development, biomass resources have gained interest for their renewability [16,17]. Tung oil is an industrial vegetable-based high-quality drying oil; it is produced from seeds of the tung tree by mechanical pressing [18]. At present, nearly 80% of the world's annual output of tung oil, which can be as high as 100,000 tons, comes from China [19]. The main component of tung oil is tung acid glyceride (octadecyl conjugated-9,11,13-trienoic acid glyceride), which accounts for 77-82% of the content of tung oil [20]. The conjugated triene bonds and ester group exhibit strong reactivity and can undergo various reactions including amidation, transesterification, Friedel-Crafts, Diels-Alder, epoxidation, and click reactions [21]. Through these reactions, tung oil has been developed into a range of products, including polyurethane foams [2], epoxy resins [22], unsaturated co-esters [23], and plasticizers [24]. To the best of our knowledge, the literature contains no studies reporting the application of tung oils to synthesize flame retardants for toughening PFs.

In this study, a novel reactive phosphorus-containing tung-oil-based derivative was designed and synthesized. First, tung oil was used to aminolytically react with diethylenetriamine to synthesize *N*-tungacyl diethylenetriamine (TA) [25]; triazine cyclophosphate (PC) was then synthesized via a quintessential Arbuzov reaction between triethyl phosphite and cyanuric chloride [26]. Phosphorus-containing tung-oil-based chemical (TAPC) was synthesized as retardants from the TA and PC [27]. Scheme 1 shows the synthetic route of the modified PFs. The chemical structures of the TA, PC, and TAPC were characterized by Fourier transform infrared (FT-IR) spectroscopy,  $^1\text{H}$  nuclear magnetic resonance (NMR) spectrometry, and  $^{31}\text{P}$  NMR spectrometry. PFs toughened with different TAPC contents were prepared by Friedel-Crafts reaction of C=C with phenol [28]. Electromechanical universal testing machines, a scanning electron microscope, thermogravimetric analyzer, and an oxygen index tester were used to investigate the mechanical properties, cell morphology, thermal stability, and flame retardancy, respectively.



**Scheme 1.** Synthetic Route of TA, PC, TAPC and modified PF.

## 2 Experimental Section

### 2.1 Materials

Triethyl phosphite, n-hexane, n-pentane, anhydrous ether, anhydrous ethanol, toluene, diethylenetriamine, phenol, tween-80, sodium methoxide (30 wt% in methanol), tetrafluoroboric acid (40 wt% in water), cyanuric chloride, polyformaldehyde, NaOH,  $\text{Na}_2\text{SO}_4$  were purchased from Shanghai Titan Scientific Co., Ltd. All raw materials were analytically pure and used as received. Tung oil was provided by the Nanjing Daziran Fine chemicals Co. Ltd ( $\geq 95\%$ ).

## 2.2 Synthesis of TA

Tung oil (100 g, ~ 0.343 mol ester group), diethylenetriamine (72.2 g, 0.7 mol), and toluene (100 mL) were charged into a 500 mL four-necked flask equipped with a mechanical stirrer and purged with nitrogen in a 100°C oil bath for 30 min. Sodium methoxide (1.5 mL, 0.008 mol) was then added to the mixture. The solution was kept stirring at 80°C for 4 h. The crude product was washed five times with distilled water before being dried over Na<sub>2</sub>SO<sub>4</sub>. After filtration and removal of the solvent under reduced pressure, a pale-brown viscous semisolid product was obtained in 92.5% yield. The total amine value was 317 mgKOH/g.

## 2.3 Synthesis of PC

Cyanuric chloride (92 g, 0.5 mol) was charged to a 500 mL four-necked flask equipped with an agitator, thermometer, dropping funnel, and reflux condenser. Then, triethyl phosphite (282 g, 1.7 mol) was added slowly with stirring at room temperature; the slow addition was necessary because the reaction is highly exothermic. The temperature for the addition of the first two-thirds of the triethyl phosphite was maintained below 50°C; the temperature during the addition of the last one-third of the triethyl phosphite was maintained below 60°C. After the triethyl phosphite addition was completed, the temperature increased to 70°C and the reaction was allowed to proceed for 4 h until no gas was released. A slight excess of triethyl phosphite was recovered by distillation under reduced pressure, and the residue was recrystallized with ethanol to yield a white solid. The yield was 84.7%.

## 2.4 Synthesis of TAPC

To the clarified solution of PC (151.5 g, 0.31 mol) in absolute ethanol (200 mL) was added an anhydrous ethanol solution (100 mL) of TA (36.4 g, 0.1 mol) dropwise with stirring at room temperature over a period of 4 h. After the addition was completed, the reaction was continued at room temperature for 24 h. Ethanol and the phosphite diester byproduct were removed by distillation under reduced pressure. The crude product was dissolved in anhydrous ethyl ether and allowed to stand in a refrigerator for 24 h to precipitate unreacted PC; the filtrate was then collected by rapid filtration. After the solvent was removed under reduced pressure, a brown viscous liquid product was obtained. The yield was 90.1%.

## 2.5 Synthesis of PFs

First, phenol, TAPC (in a ratio of 5, 10, or 15 wt% relative to the phenol), and 1 wt% tetrafluoroboric acid were added to a 500 mL four-necked flask equipped with a thermocouple, mechanical stirrer, and condenser. The mixture was stirred at 90°C for 2 h and then cooled to 70°C. Second, paraformaldehyde was poured into the resulting system in multiple portions (the depolymerization releases a large amount of heat); the pH was maintained at 9-10 by the addition of an aqueous sodium hydroxide solution (30 wt%). The system was maintained at 70°C for 2 h and then heated to 92°C for 1 h. The pure PF was prepared via the same process but without TAPC. Third, the previously prepared phenolic resin (100 g), polysorbate-80 (4 g), and n-pentane (6 g) were mixed for 30 s under rapid stirring at 2000 rpm. p-Toluenesulfonic acid aqueous solution (20 g, 65 wt%) was added rapidly with stirring at 2000 rpm for 30 s. Finally, the mixture was quickly poured into a stainless steel mold (200 mm × 200 mm × 50 mm) at 80°C and allowed to stand for 60 min. The samples were labeled according to their TAPC loading level; for instance, the foam containing 5 wt% TAPC was labeled “PF-5”.

## 2.6 Characterizations

FT-IR spectroscopy experiments were performed on a Nicolet IS 10 FT-IR spectrometer (Nicolet Co., USA) in the range of 4000~500 cm<sup>-1</sup> and the resolution of 4 cm<sup>-1</sup>. <sup>1</sup>H NMR and <sup>31</sup>P NMR spectra were confirmed by a Bruker ARX 300 nuclear magnetic resonance spectrometer with CDCl<sub>3</sub> and DMSO-d<sub>6</sub> as the solvent and tetramethylsilane as the internal standard. Thermogravimetric analyzer (TGA) measurements were performed NETZSCH TG 209F1 (Netzsch Instrument Crop., Germany) in a nitrogen atmosphere was used with a heating rate of 20 °C/min and a temperature range of 35-800°C. The

morphology of foam was examined with a JSM-7600F (JEOL, Japan) scanning electron microscopy (SEM) with an accelerating voltage of 15 kV after gold sputtering.

The total amine value is defined as the number of milligrams of potassium hydroxide (mgKOH/g) converted into the amount of acid required to neutralize 1 g of sample. We determined the total amine value according to ZBG71005-89; the titration reaction was:



Total amine value  $S$  (mgKOH/g) was calculated according to the Eq. (1):

$$S = \frac{c \times V \times 56.11}{m} \quad (1)$$

where  $c$  was the concentration (mol/L) of perchloric acid-glacial acetic acid standard solution,  $V$  was the volume (mL) of perchloric acid-glacial acetic acid standard solution consumed,  $m$  was the accurate quality (g) of the sample, 56.11 was the molar mass (g/mol) of KOH.

Mechanical properties of the foams were measured by a CMT4000 universal testing machine. Each specimen used for the flexural strength test was 120 mm  $\times$  25 mm  $\times$  20 mm (according to GB/T8812.1-2007) and the compressive strength test was 50 mm  $\times$  50 mm  $\times$  50 mm (according to GB/T 8813-2008). In both measurements, each named sample need test at least three times. The density was determined according to the mass of the foam and the dimensions.

Limiting oxygen index (LOI) of foam was performed according to GB/T 2406-1993 standard on the JF-3 oxygen index tester (Nanjing Jiangning Analytical Instrument Factory, China). The size of the samples was 150 mm  $\times$  10 mm  $\times$  10 mm.

### 3 Results and Discussion

#### 3.1 Synthesis and Characterization of TA, PC, and TAPC

TA was synthesized by an aminolysis reaction of tung oil with diethylenetriamine. In the FT-IR spectrum of TA (Fig. 1(a),I), characteristic peaks are observed at approximately 3287  $\text{cm}^{-1}$  and 1555  $\text{cm}^{-1}$ ; these peaks are attributed to N-H stretching and bending vibrations, respectively. Additional peaks at 1642  $\text{cm}^{-1}$  and 1129  $\text{cm}^{-1}$  are attributed to C=O and C-N, respectively. Fig. 2 shows the FT-IR spectra for samples collected at different times (0.5, 1, 2, 4, and 5 h) during the synthesis of TA, along with the spectrum of tung oil for comparison. With increasing reaction time, the stretching and bending vibrations of N-H and the C=O characteristic peak of amide gradually increased in intensity, whereas the intensity of the C=O characteristic peak at 1742  $\text{cm}^{-1}$  of the ester group gradually decreases. The total amine value of TA was 317 mgKOH/g, and the relative error with the theoretical value (308 mgKOH/g) was 2.9%. All of these results confirm the successful synthesis of TA.

In the  $^1\text{H}$  NMR spectrum of TA (Fig. 1(b)), the single peak at 0.87 ppm is assigned to the protons of the methyl group. The peaks in the range 5.33-6.10 ppm correspond to the protons of the carbon-carbon double bonds. The peak at 7.88 ppm is attributed to the proton of O=C-NH. PC was synthesized by a quintessential arbusov reaction between triethyl phosphite and cyanuric chloride. In the FT-IR spectrum of the PC (Fig. 1(a),II), absorption peaks observed at 1679  $\text{cm}^{-1}$  are attributed to the skeleton vibration of the triazine ring. Peaks at 1495  $\text{cm}^{-1}$  belong to the C=N stretching vibration, strong peaks at 1252  $\text{cm}^{-1}$  represent P=O, and peaks at 1013  $\text{cm}^{-1}$  and 975  $\text{cm}^{-1}$  are attributed to P-O and C-O bonds, respectively. The characteristic peaks of the C-P condensation bond appear at 749  $\text{cm}^{-1}$  [29]. In the  $^1\text{H}$  NMR spectrum of PC (Fig. 1(c)), the multiplet peaks at 1.35 ppm correspond to the protons of the methyl group, and the multiplet peaks at 4.31 ppm belong to the protons of the methylene group.

TAPC was the retardant synthesized from the TA and PC. In the FT-IR spectrum of TAPC (Fig. 1(a), III), the peaks of N-H almost disappear and a new peak appears at  $1529\text{ cm}^{-1}$  belonging to C (triazine ring)-N. Fig. 1(d) shows the  $^1\text{H}$  NMR spectrum of TAPC. The peaks attributable to the protons of the carbon-carbon double bonds shift to lower frequencies (ca. 4.70-6.00 ppm). Signals at approximately 1.30-1.70 ppm corresponding to the protons of methylene and methyl groups appear; these peaks are derived from the TA and PC. When the total amine value of TAPC was measured, discoloration of the solution was not observed when the bromophenol blue indicator (that was blue in dilute alkali solution) was added dropwise to the sample. These results thus support the successful synthesis of TAPC.

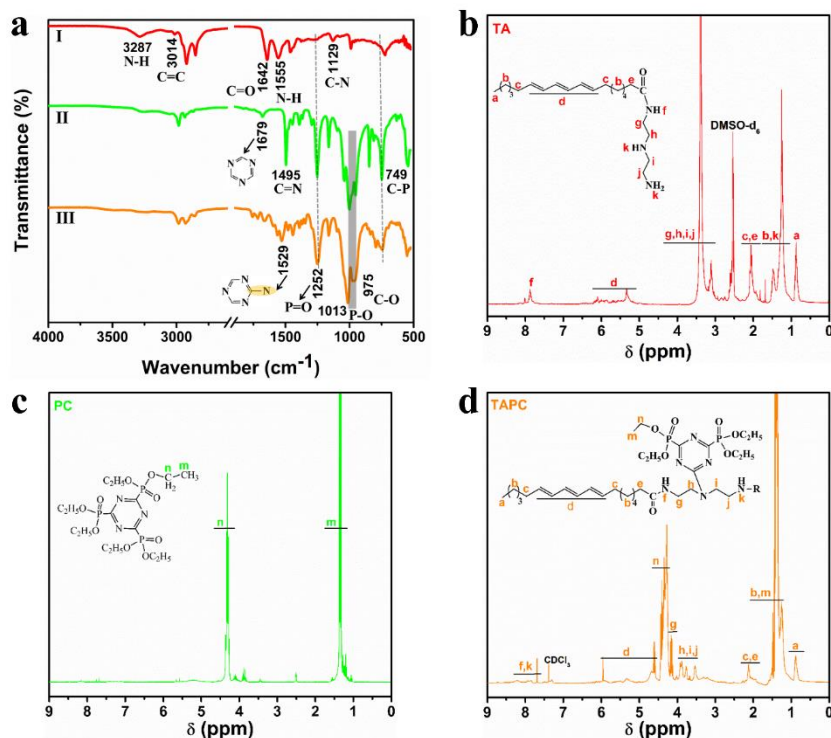


**Figure 1:** a. FT-IR spectra of TA (I), PC (II), TAPA (III). b.  $^1\text{H}$  NMR spectra of TA. c.  $^1\text{H}$  NMR spectra of PC. d.  $^1\text{H}$  NMR spectra of TAP

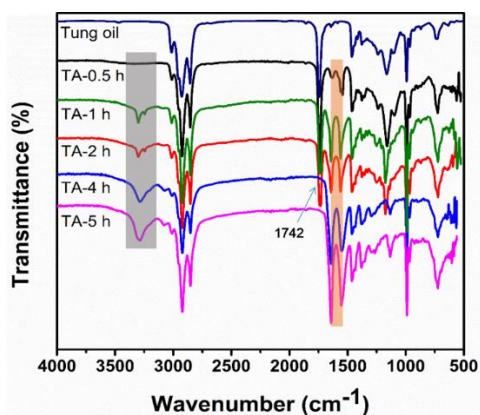


**Figure 2:** The FT-IR spectra at a different time (0.5, 1, 2, 4, 5 h) during the synthesis of TA and comparison with the tung oil

### 3.2 Characterization of PFs

#### 3.2.1 Mechanical Properties

The mechanical properties of the pure and TAPC-modified PFs were determined via static compressive tensile tests and flexural tests. These results and the apparent densities of the samples are summarized in Tab. 1. The compressive and flexural tests were performed by measuring four equal samples at a testing rate of  $10 \text{ mm min}^{-1}$  at room temperature. As shown in Fig. 3(a), the addition of TAPC substantially improved the mechanical properties of the foam. The compressive and flexural strength of the pure PF was 0.16 MPa and 0.24 MPa, respectively. With increasing TAPC content, the compressive and flexural strength of the modified foams showed a trend of first increasing and then decreasing. The modified foam PF-10 exhibited maximum compressive and flexural strengths of 0.265 MPa and 0.57 MPa, respectively, which represent increases of 65.63% and 137.5%, respectively, compared with those of the unmodified pure PF. This enhancement is attributed to the rigid backbone of the phenolic resin being bonded with the long aliphatic chain of the TAPC via the Friedel-Crafts reaction, which introduces a soft chain into the backbone and increases the alkyl side-chain length. A high level of sterically hindered PC is attached to the alkyl side chain, which is detrimental to the reaction between formaldehyde and phenol during the formulation and the intermolecular polycondensation during the curing process. Excessive TAPC instead causes the compressive and flexural strength of the modified foam to decrease.

To avoid the adverse effect of the apparent density of PFs on their mechanical properties, we further evaluated the specific compressive and flexural strengths (strength/density) of the PFs. As depicted in Fig. 3(b), the specific strength exhibited a change similar to that of the strength. The specific compressive and flexural strengths of pure PF were 2.98 MPa and 4.47 MPa, respectively. The modified foam PF-10 showed maximum specific compressive and flexural strengths of 5.67 MPa and 12.46 MPa, respectively, which represent increases of 90.67% and 178.7%, respectively, compared with the corresponding strengths of the unmodified pure PF. These results strongly demonstrate the toughening effect of TAPC on the foam and indicate that an optimal content of TAPC exists that best improves the mechanical properties of PFs.

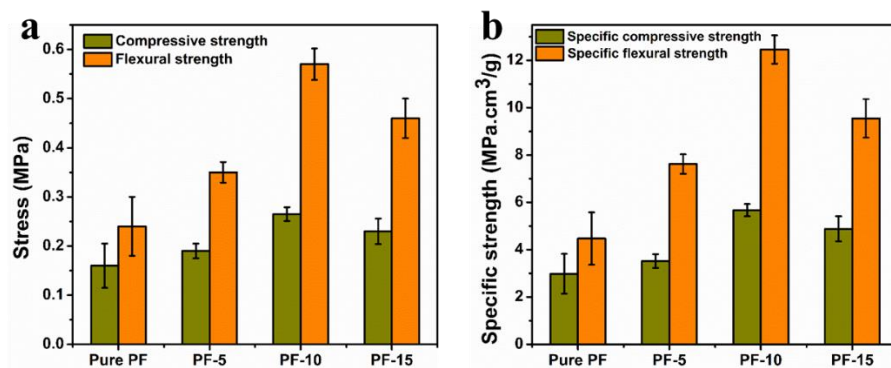


**Figure 3:** a. Compressive and flexural strength of pure and TAPC modified PFs; b. Specific compressive and flexural strength of pure and TAPC modified PFs

**Table 1:** Mechanical properties of Pure PF and TAPC modified PFs

Samples	Density (Kg/m <sup>3</sup> )	Compressive strength (MPa)	Flexural strength (MPa)
Pure PF	53.72 ± 1.49	0.16 ± 0.045	0.24 ± 0.06
PF-5	51.20 ± 3.76	0.19 ± 0.015	0.35 ± 0.021
PF-10	52.95 ± 1.92	0.265 ± 0.014	0.57 ± 0.032
PF-15	49.22 ± 2.19	0.23 ± 0.026	0.46 ± 0.040

For foam materials, the morphology and distribution of the cells strongly influence their mechanical properties. Fig. 4 shows the microstructure of the pure PF and the TAPC-modified PFs, as observed by scanning electron microscopy (SEM), and the corresponding cell pore size distribution. We calculated the pore size of more than 100 cells in the SEM images using the software Nano Measurer 1.2. Pure PF exhibited the broadest pore size distribution range (from 62.98 to 200.03  $\mu\text{m}$ ) and the largest average value (111.41  $\mu\text{m}$ ); the regularity of the cells was poor. The TAPC-modified PFs exhibited a narrower pore size distribution, a smaller pore size average, and a more regular cell morphology than the pure PF. In particular, PF-10, with optimal mechanical properties, exhibited the narrowest pore size distribution (from 48.05 to 104.55  $\mu\text{m}$ ), the smallest average pore size (73.08  $\mu\text{m}$ ), and a nearly hexahedral cell morphology. Collectively, these results reflect the regular cell morphology and show that a smaller pore size leads to enhanced mechanical properties of the foams.

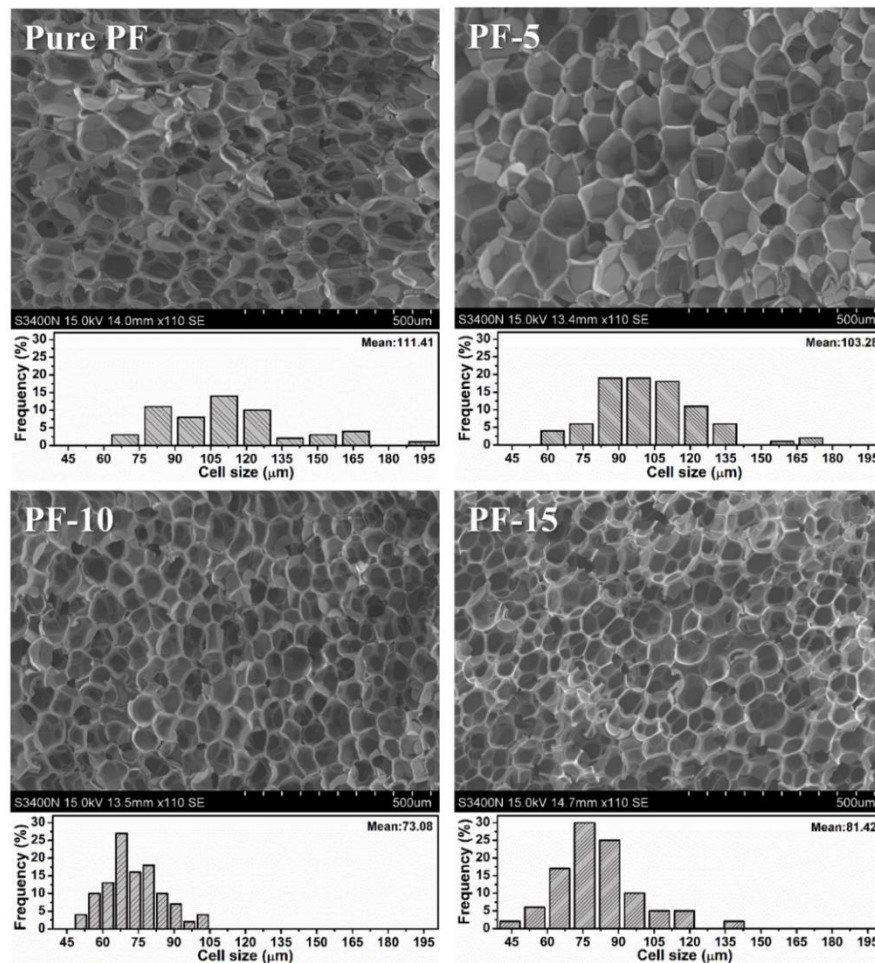


**Figure 4:** SEM and cell sizes distribution of Pure PF and TAPC modified PFs

### 3.2.2 Flame Retardant Properties

Limiting oxygen index (LOI) is an important indicator used to characterize the flame-retardant properties of materials [30,31]. The better the flame retardancy of the material, the higher its LOI; conversely, the lower LOI, the more flammable the material. Fig. 5 shows the flame-retardant properties of pure PF and TAPC-modified PF, as reflected by their LOI. As expected, the addition of TAPC enhanced the flame-retardant properties of the PF, even though the flame retardancy tended to first increase and then decrease. The LOI of pure PF was 32.10%. The LOIs for the PF-5, PF-10, and PF-15

were 35.23%, 40.83%, and 35.80%, which represent increases of 9.75%, 27.20% and 11.53%, respectively, compared with the LOI of the unmodified pure PF. The phosphorus-containing compound forms  $\text{PO}\cdot$  during polymer combustion, which can remove  $\text{H}\cdot$  and  $\text{OH}\cdot$  generated during combustion to suppress the rapid control step of flame propagation, i.e., the chain-branching reaction, thereby suppressing the flame [9,32]. Meanwhile,  $\text{PO}\cdot$  absorbs  $\text{H}\cdot$  and  $\text{OH}\cdot$  to form phosphoric acid, which can act as a dehydrating agent to promote the formation of a carbonized layer [33,34]. However, the tung-oil-based flexible long chain is flammable, which competes with the flame-retardant phosphorus component. Under the combined action of flame-retardant phosphorus and flammable flexible long chains, there is an optimum content of TAPC that best improves the flame retardancy of the PFs.

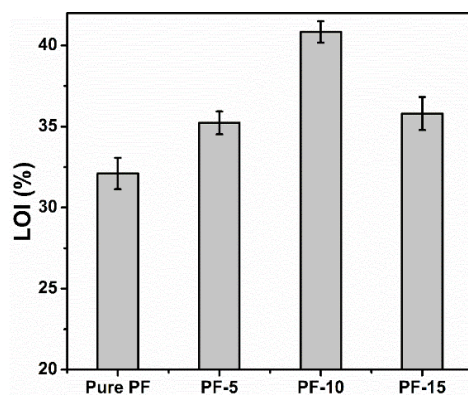


**Figure 5:** LOIs of Pure PF and TAPC modified PFs

### 3.3.3 Thermogravimetric Analysis

Fig. 6 shows the thermogravimetric analysis (TGA) and differential thermogravimetry (DTG) curves of pure PF and TACP-modified PFs, as recorded with the samples under a nitrogen/air atmosphere; the data relevant to degradation  $T_{\max}$  and residual mass are listed in Tab. 2. As shown in Fig. 6(a), three distinct stages of thermal decomposition were observed for all of the foams decomposed under a nitrogen atmosphere. The initial stage of thermal mass loss associated with the release of water with  $\sim 5\%$  mass loss occurred at 40-200°C; it was attributed mainly to unreacted phenol and formaldehyde as well as to the blowing agent [9]. The second stage at approximately 200-400°C resulted from the decomposition of surfactant and to breakage of the ether bonds formed during the curing of the resin into a more stable bridging bond; this process is accompanied by water release, resulting in a substantial increase in the mass-loss rate [35]. The third stage (approximately 400-800°C) was the main process of thermal mass loss [36]. During this process, the methylene-bridged structure and the long-chain molecules degraded to form low-molecular-mass products. As the TAPC content was increased (from pure PF to PF-15), the initial decomposition temperature ( $T_{-5\%}$ , the temperature required for 5% mass loss) increased (from 174.9 to 206.7°C). As shown in Fig. 6(b), four distinct stages of thermal decomposition were observed for all of the foams decomposed in air. The TAPC-modified foams exhibited a lower rate of thermal decomposition than the pure PF, with PF-10 exhibiting the lowest rate. Meanwhile, the initial decomposition temperature of the TAPC-modified foams increased by approximately 90°C. Moreover, the residual mass of the TAPC-modified foams also increased substantially, by approximately 10%. All of these results indicate that TAPC enhances the thermal stability of the foam, especially in an air atmosphere. This TAPC-induced enhancement of N and P flame-retardant elements forms an insulating carbonized layer during thermal degradation [37,38]. As a barrier, the carbon layer can slow the transfer of heat to the inner layer and air intrusion, thus improving the flame retardancy and thermal stability of the foam [39,40].

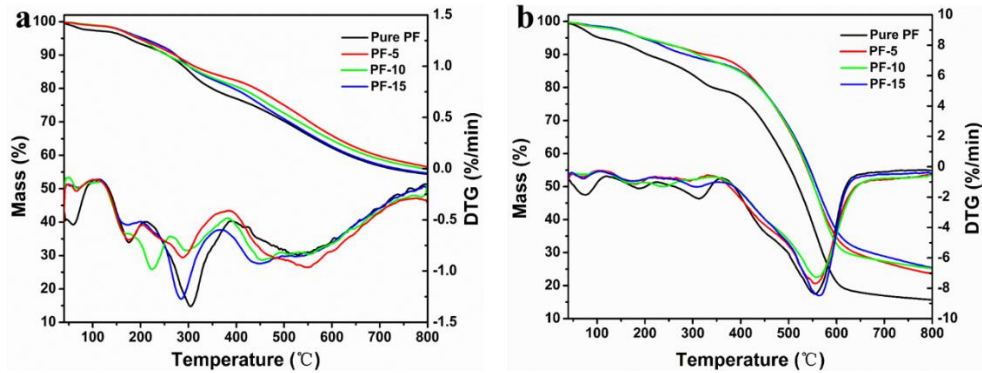


**Figure 6:** TGA and DTG curves of Pure PF and TAPC modified PFs in N<sub>2</sub> (a)/air (b) atmosphere

**Table 2:** TGA data of Pure PF and TAPC modified PFs in N<sub>2</sub> (a)/air (b) atmosphere

Samples	Density		T <sub>max</sub> (°C)			Residual mass (%)	
	(Kg/m <sup>3</sup> )	T <sub>-5%</sub> (°C)	Step II	Step III	Step IV		
N <sub>2</sub>	Pure PF	53.72 ± 1.49	174.9	305.1	528.9	/	54.41
	PF-5	51.20 ± 3.76	196.5	288.3	549.5	/	56.54
	PF-10	52.95 ± 1.92	196.7	298.6	454.0	/	55.82
	PF-15	49.22 ± 2.19	206.7	284.6	447.5	/	54.64
Air	Pure PF	-	106.3	186.7	312.4	556.4	15.73
	PF-5	-	195.7	181.8	293.5	555.9	23.62
	PF-10	-	196.5	/	/	556.9	25.41
	PF-15	-	199.1	173.9	306.9	565.1	25.19

#### 4 Conclusions

We synthesized novel reactive tung-oil-based flame retardants as a toughener for toughening PFs. The TAPC-modified PFs display improved compressive strength and flexural strength. The microstructure observed by SEM showed that the TAPC-modified PFs possessed a more uniform cell morphology, a narrower pore size distribution range, and a smaller average pore size than unmodified PFs to ensure improved mechanical properties. Specifically, the mechanical properties of the PFs modified by the addition of 10 wt% of TAPC increased 90.67% in specific compressive strength and 178.7% in specific flexural strength. The addition of TAPC improved the flame-retardant properties of the foam, resulting in an LOI as high as 40.83% (an increase in 27.20% compared with that of pure PF). This work demonstrates the preparation of a thermal insulation foam with excellent mechanical and flame-retardant properties through modification using biomass-derived materials. This approach promotes the development of environmentally friendly and advanced materials via renewable biomass.

**Acknowledgments:** The authors are grateful to the financial support from the Fundamental Research Funds for the Central Non-profit Research Institution of CAF (No. CAFYBB2018MA001).

#### References

- Özkan, D. B., Onan, C. (2011). Optimization of insulation thickness for different glazing areas in buildings for various climatic regions in Turkey. *Applied Energy*, 88(4), 1331-1342.
- Zhou, W., Bo, C., Jia, P., Zhou, Y., Zhang, M. (2019). Effects of tung oil-based polyols on the thermal stability,

- flame retardancy, and mechanical properties of rigid polyurethane foam. *Polymers*, 11(1), 45.
3. Stec, A. A., Hull, T. R. (2011). Assessment of the fire toxicity of building insulation materials. *Energy and Buildings*, 43(2-3), 498-506.
  4. Liang, B., Li, X., Hu, L., Bo, C., Zhou, J. et al. (2016). Foaming resol resin modified with polyhydroxylated cardanol and its application to phenolic foams. *Industrial Crops and Products*, 80, 194-196.
  5. Bo, C., Hu, L., Chen, Y., Yang, X., Zhang, M. et al. (2018). Synthesis of a novel cardanol-based compound and environmentally sustainable production of phenolic foam. *Journal of Materials Science*, 53(15), 10784-10797.
  6. Hu, L., Zhou, Y., Liu, R., Zhang, M., Yang, X. (2013). Synthesis of foaming resol resin modified with oxidatively degraded lignosulfonate. *Industrial Crops and Products*, 44, 364-366.
  7. Guo, Y., Hu, L., Bo, C., Shang, Q., Feng, G. et al. (2018). Mechanical property of lignin-modified phenolic foam enhanced by nano-SiO<sub>2</sub> via a novel method. *Chemical Papers*, 72(3), 763-767.
  8. Yang, C., Zhuang, Z. H., Yang, Z. G. (2014). Pulverized polyurethane foam particles reinforced rigid polyurethane foam and phenolic foam. *Journal of Applied Polymer Science*, 131(1).
  9. Bo, C., Wei, S., Hu, L., Jia, P., Liang, B. et al. (2016). Synthesis of a cardanol-based phosphorus-containing polyurethane prepolymer and its application in phenolic foams. *RSC Advances*, 6(67), 62999-63005.
  10. Liu, L., Fu, M., Wang, Z. (2015). Synthesis of boron-containing toughening agents and their application in phenolic foams. *Industrial & Engineering Chemistry Research*, 54(7), 1962-1970.
  11. Yu, Z., Li, J., Yang, L., Yao, Y., Su, Z. et al. (2012). Synthesis and properties of nano carboxylic acrylonitrile butadiene rubber latex toughened phenolic resin. *Journal of Applied Polymer Science*, 123(2), 1079-1084.
  12. Gao, M., Wu, W., Wang, Y., Wang, Y., Wang, H. (2016). Phenolic foam modified with dicyandiamide as toughening agent. *Journal of Thermal Analysis and Calorimetry*, 124(1), 189-195.
  13. Yuan, H., Xing, W., Yang, H., Song, L., Hu, Y. et al. (2013). Mechanical and thermal properties of phenolic/glass fiber foam modified with phosphorus-containing polyurethane prepolymer. *Polymer International*, 62(2), 273-279.
  14. Yang, H., Wang, X., Yuan, H., Song, L., Hu, Y. et al. (2012). Fire performance and mechanical properties of phenolic foams modified by phosphorus-containing polyethers. *Journal of Polymer Research*, 19(3), 9831.
  15. Yang, H., Wang, X., Yu, B., Yuan, H., Song, L. et al. (2013). A novel polyurethane prepolymer as toughening agent: preparation, characterization, and its influence on mechanical and flame retardant properties of phenolic foam. *Journal of Applied Polymer Science*, 128(5), 2720-2728.
  16. Laurichesse, S., Avérous, L. (2014). Chemical modification of lignins: Towards biobased polymers. *Progress in Polymer Science*, 39(7), 1266-1290.
  17. Zhu, Y., Romain, C., Williams, C. K. (2016). Sustainable polymers from renewable resources. *Nature*, 540(7633), 354.
  18. Meiorin, C., Aranguren, M. I., Mosiewicki, M. A. (2015). Polymeric networks based on tung oil: reaction and modification with green oil monomers. *European Polymer Journal*, 67, 551-560.
  19. Sharma, V., Das, L., Pradhan, R. C., Naik, S. N., Bhatnagar, N. et al. (2011). Physical properties of tung seed: an industrial oil yielding crop. *Industrial Crops and Products*, 33(2), 440-444.
  20. Huang, K., Liu, Z., Zhang, J., Li, S., Li, M. N. et al. (2014). Epoxy monomers derived from tung oil fatty acids and its regulable thermosets cured in two synergistic ways. *Biomacromolecules*, 15(3), 837-843.
  21. Jia, P., Ma, Y., Xia, H., Zheng, M., Feng, G. et al. (2018). Clean synthesis of epoxidized tung oil derivatives via phase transfer catalyst and thiol-ene reaction: a detailed study. *ACS Sustainable Chemistry & Engineering*, 6(11), 13983-13994.
  22. Huang, K., Liu, Z., Zhang, J., Li, S., Li, M. et al. (2015). A self-crosslinking thermosetting monomer with both epoxy and anhydride groups derived from tung oil fatty acids: synthesis and properties. *European Polymer Journal*, 70, 45-54.
  23. Liu, C., Shang, Q., Jia, P., Dai, Y., Zhou, Y. et al. (2016). Tung oil-based unsaturated co-ester macromonomer for thermosetting polymers: synergetic synthesis and copolymerization with styrene. *ACS Sustainable Chemistry & Engineering*, 4(6), 3437-3449.
  24. Chen, J., Wang, Y., Huang, J., Li, K., Nie, X. (2017). Synthesis of tung-oil-based triglycidyl ester plasticizer and its effects on poly (vinyl chloride) soft films. *ACS Sustainable Chemistry & Engineering*, 6(1), 642-651.

25. Song, F., Li, Z., Jia, P., Zhang, M., Bo, C. et al. (2019). Tunable “soft and stiff”, self-healing, recyclable, thermadapt shape memory biomass polymers based on multiple hydrogen bonds and dynamic imine bonds. *Journal of Materials Chemistry A*, 7(21), 13400-13410.
26. Wang, Y., Diao, J., Wang, D., Ji, X. (2010). Solvent-free Synthesis of 2, 4, 6-Tri (O, O-dimethylphosphoryl)-1, 3, 5-triazine. *Chemical World*, 51(5), 298-300.
27. Gang, L., Shumei, L., Qi, S., Jianqing, Z., Yonghua, Z. et al. (2007). Synthesis and characterization of phosphorus-containing triazine polymer. *Petrochemical Technology*, 36(2), 173-177.
28. Ionescu, M., Petrovic, Z. (2011). Phenolation of vegetable oils. *Journal of the Serbian Chemical Society*, 76(4), 591-606.
29. Wang, H., Niu, H., Dong, J. (2017). Inherently flame retardant polypropylene copolymer. *Polymer*, 126, 109-115.
30. Bo, C., Hu, L., Jia, P., Liang, B., Zhou, J. et al. (2015). Structure and thermal properties of phosphorus-containing polyol synthesized from cardanol. *RSC Advances*, 5(129), 106651-106660.
31. Suzanne, M., Delichatsios, M. A., Zhang, J. P. (2014). Flame extinction properties of solids obtained from limiting oxygen index tests. *Combustion and Flame*, 161(1), 288-294.
32. Qian, L., Ye, L., Qiu, Y., Qu, S. (2011). Thermal degradation behavior of the compound containing phosphaphenanthrene and phosphazene groups and its flame retardant mechanism on epoxy resin. *Polymer*, 52(24), 5486-5493.
33. Jia, P., Zhang, M., Hu, L., Bo, C., Zhou, Y. (2015). Thermal degradation and flame retardant mechanism of poly (vinyl chloride) plasticized with a novel chlorinated phosphate based on soybean oil. *Thermochimica Acta*, 613, 113-120.
34. Ding, H., Wang, J., Wang, C., Chu, F. (2016). Synthesis of a novel phosphorus and nitrogen-containing bio-based polyols and its application in flame retardant polyurethane sealant. *Polymer Degradation and Stability*, 124, 43-50.
35. Sui, X., Wang, Z. (2013). Flame-retardant and mechanical properties of phenolic foams toughened with polyethylene glycol phosphates. *Polymers for advanced technologies*, 24(6), 593-599.
36. Ma, Y., Wang, J., Xu, Y., Wang, C., Chu, F. (2013). Preparation and characterization of phenolic foams with eco-friendly halogen-free flame retardant. *Journal of Thermal Analysis and Calorimetry*, 114(3), 1143-1151.
37. Jia, P., Hu, L., Feng, G., Bo, C., Zhou, J. et al. (2017). Design and synthesis of a castor oil based plasticizer containing THEIC and diethyl phosphate groups for the preparation of flame-retardant PVC materials. *RSC Advances*, 7(2), 897-903.
38. Yadav, R., Srivastava, D. (2010). Blends of cardanol-based epoxidized novolac resin and CTBN for application in surface coating: a study on thermal, mechanical, chemical, and morphological characteristics. *Journal of Coatings Technology and Research*, 7(5), 557-568.
39. Jia, P., Hu, L., Zhang, M., Feng, G., Zhou, Y. (2017). Phosphorus containing castor oil based derivatives: potential non-migratory flame retardant plasticizer. *European Polymer Journal*, 87, 209-220.
40. Jia, P., Zhang, M., Liu, C., Hu, L., Feng, G. et al. (2015). Effect of chlorinated phosphate ester based on castor oil on thermal degradation of poly (vinyl chloride) blends and its flame retardant mechanism as secondary plasticizer. *RSC Advances*, 5(51), 41169-41178.